Fast decolorization of azo dyes in both alkaline and acidic solutions by Al-based metallic glasses

Peipei Wang [a, b], Jun-Qiang Wang [a, *], He Li [c], Hao Yang [a, d], Juntao Huo [a], Jianguo Wang [d], Chuntao Chang [a], Xinmin Wang [a], Run-Wei Li [a], Gang Wang [b, **]

[a] Key Laboratory of Magnetic Materials and Devices & Zhejiang Province Key Laboratory of Magnetic Materials and Application Technology, Ningbo Institute of Materials Technology & Engineering, Chinese Academy of Sciences, Ningbo, Zhejiang, 315201, China
[b] School of Materials Science and Engineering, Shanghai University, Shanghai, 200444, China
[c] Ningbo Institute of Materials Technology & Engineering, Chinese Academy of Sciences, Ningbo, Zhejiang, 315201, China
[d] School of Materials Science and Engineering, Anhui University of Technology, Maanshan, Anhui, 243032, China

ARTICLE INFO

ABSTRACT

The advanced efficiency of metallic glasses in degrading organic water pollutants has attracted wide interests. Yet the decolorization efficiency decreases in alkaline solutions which remains a challenge for their application. In this work, the performance of $Al_{91-x}Ni_9Y_x$ (x = 0, 3, 6, 9 at.%) metallic ribbons in degrading azo dye in aqueous solutions at wide pH conditions is studied. It is surprising to find that the reaction activity of Al-based metallic glass in alkaline and acidic azo dye solution is about 1.5 and 189 times higher than that in neutral solutions, respectively. The low reaction activation energy and formation of nano-porosity on the surface of metallic glass are responsible for the high reactivity in alkaline and acidic solutions. The reaction activity can be further enhanced by modifying the alloy composition. These findings suggest that the Al-based metallic glasses hold promising potential in degrading azo dyes solutions, especially in alkaline and acidic environments.

1. Introduction

Metallic glasses, unlike the crystalline alloys that are thermodynamically equilibrated, are metastable materials in far-from-equilibrium states [1,2]. The far-from-equilibrium nature bestows metallic glasses many excellent properties that are unachievable in crystalline alloys [3—5]. The advanced properties make metallic glasses promising candidates as functional materials, such as catalysts [6—9], biomaterials [10—15], soft magnetic materials [16,17], and magnetocaloric effects [18,19]. It was found recently that Fe-Si-B and Fe-Si-B-Mo amorphous alloys can degrade Acid Orange II azo dye solutions [20,21]. The reactivity of amorphous alloys is higher than their crystalline counterparts and commercial Fe powders. This functional application of metallic glasses holds promising application potentials because of its higher reactivity, lower cost, and easier manipulations than many other methods, such as physical adsorption [22], nanoscale bimetallic particles [23] and bacterial degradation [24]. Extensive efforts have been devoted to exploring new compositions with advanced properties and to studying the reaction mechanisms. Fe-B binary amorphous alloy can degrade Direct Blue 6 by about 1.8 and 89 times faster than its crystalline counterpart and commercial Fe powders, respectively [25]. The low reaction activation energy (25.4 kJ/mol) is thought to be responsible for the high reaction activity. The boron contributes to make the surface oxide layer loose to allow ions exchange between alloy and solution. Addition of Nb into Fe-Si-B metallic glasses can further increase the reactivity in degrading Direct Blue 6 [7]. The reactivity of Fe-Si-B-Nb metallic glass powders is about 200 times higher than commercial Fe powders. The reactivity of Fe-Si-B-Y metallic glass powders is about 1000 times higher than commercial Fe powders in degrading Methyl Orange and remain stable after 13 cycles [26]. The weak atomic bonds as a result of cluster competition may be responsible for the high reactivity of Fe-B-Y metallic glass in degrading Orange G [27].

Besides Fe-based metallic glasses, efforts have also been devoted to looking for new metallic glasses that can degrade organic water contaminants. Mg-Zn-Ca metallic glasses exhibit about 1000 times higher reactivity compared to commercial Fe powders in degrading

---

* Corresponding author.
** Corresponding author.
  E-mail addresses: jqwang@nimte.ac.cn (J.-Q. Wang), g.wang@shu.edu.cn (G. Wang).
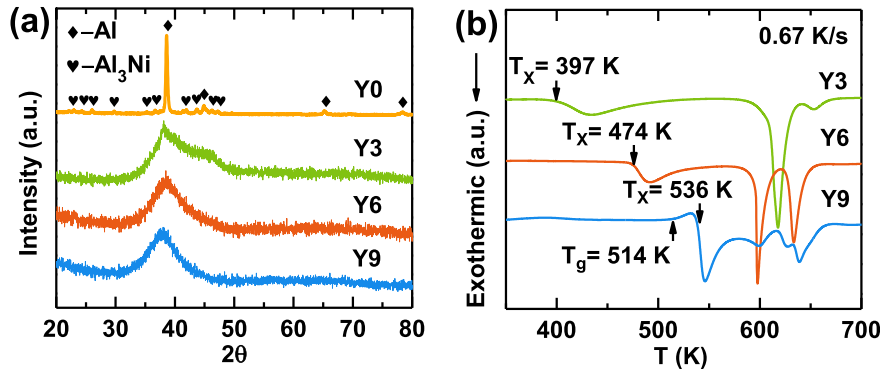
Fig. 1. (a) XRD and (b) DSC curves of the Al-Ni-Y ribbons confirm the atomic structure.

Direct Blue 6 [8]. Increasing the concentration of Zn decreases the reactivity [28,29]. Partially amorphous Mg-Zn-Ca powders can also exhibit superior reaction efficiency in degrading Congo red dye [30]. Co-based and Al-based metallic glasses are also reported to be able to degrade azo dyes efficiently [31,32]. Surface decoration by nanopores and oxides is demonstrated to be able to further increase the reaction activity of metallic glasses in adsorbing and degrading Direct Blue 6, Phenol, and Cr^{6+} [33−35]. Photocatalytic
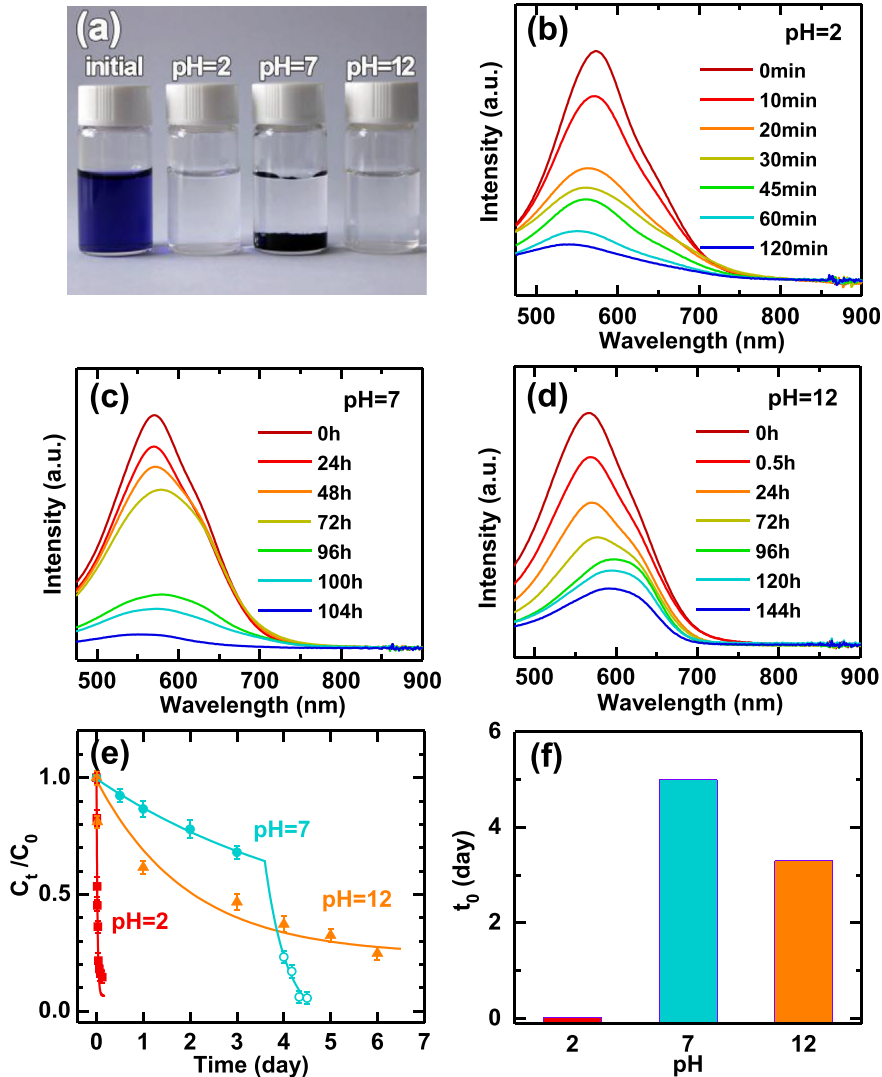

Fig. 2. (a) The appearance of DB 2B solution before and after degradation by Y6 metallic glass ribbons under different pH values at room temperature. The UV absorption spectra of DB 2B solution after different reaction time with Y6 metallic glass ribbons at (b) pH = 2, (c) 7, and (d) 12, respectively. (e) The normalized concentration of DB 2B solution after different degradation time with Y6 metallic glass ribbons. (f) The comparison of degradation time constant t_0 for different pH. For pH = 7, the t_0 is derived by fitting the data of the first stage.

method using metallic glasses and TiO_2 composite powders also exhibits higher degradation activity than pure TiO_2 in degrading Methylene Blue [36]. Using Fenton-like method, Fe-B-Si metallic glass exhibits high reactivity in degrading organic Methyl benzene, Methanol, RhB, Methyl blue, Methyl orange, and Cibacron brilliant red 3B-A [37–40]. Photon irradiation can further accelerate the Fenton-like process of Fe-B-Si metallic glass in degrading BR3B-A dye [41]. Via activating persulfate, Fe-B-Si metallic glass exhibits superior surface stability and reusability in degrading methylene blue [42]. The newly developed AlCoCrTiZn high-entropy alloy with

severe lattice distortion also exhibits a prominent efficiency in degrading Direct Blue 6 [43]. Even though there has been big progress in improving the reactivity of metallic glasses in degrading organic pollutants. One common challenge is that the reactivity decreases strikingly along with the pH increase. Since much of the dye polluted water is alkaline, it is of high interests to explore new metallic glasses that exhibit high reactivity in alkaline solutions.

In this work, we studied the reactivity of Al-Ni-Y metallic glasses in degrading Direct Blue (DB) 2B azo dye solutions. The influence of solution acidity, alloy composition, and reaction temperature has been studied. The reaction mechanism has been studied based on the evolution of surface morphologies and the compositions change for the metallic glass ribbons.

2. Experimental

2.1. Fabrication and characterization

The alloy ingots with nominal compositions of $Al_{91-x}Ni_9Y_x$ (x = 0, 3, 6, 9 at.%) were prepared by induction melting the mixtures of pure Al, Ni, Y metals under high purity argon atmosphere. The Al-Ni-Y metallic glass ribbons with a cross-section of about 1.5 mm × 0.03 mm were fabricated by single roller melt-spinning method under the protection of argon atmosphere. The surface speed of spinning roller is 35 m/s. The atomic structure of the ribbons was verified by X-ray diffraction (XRD, Bruker D8 Advance) with Cu $K\alpha$ radiation. The amorphous structure of the ribbons was also certified by differential scanning calorimetry (DSC, NETZSCH 404C) at a heating rate of 0.67 K/s.

2.2. Reactivity measurements

Commercially available azo dye ($C_{32}H_{20}N_6Na_4O_{14}S_4$) powders were purchased from Shanghai East Lion Silk Screen Printing Ink Co., Ltd. 200 mg/L dye solution was prepared by dissolving the azo dye powders with deionized water. The acidity of the solutions was tuned by adding 1 M HCl solution or 0.1 M NaOH solution. For each time, 70 ml DB 2B solution was put into the 100 mL beaker for reaction test. The temperature was controlled by water-bath device. The Al-Ni-Y metallic glass ribbons were cut into small parts with a size of 10 mm × 1.5 mm × 0.03 mm. The specific surface area of the ribbons is 0.022, 0.023, 0.022, 0.024 m^2/g for $Al_{91}Ni_9$ (Y0), $Al_{88}Ni_9Y_3$ (Y3), $Al_{85}Ni_9Y_6$ (Y6), $Al_{82}Ni_9Y_9$ (Y9), respectively. Then, they were put into the solution with a ratio of 13.3 g/L. The solution was not stirred during reaction. 2 mL solution was taken out each time for test. To evaluate the degradation activity, the concentration decay of solution was monitored by ultraviolet-visible absorption spectrophotometer (Perkin-Elmer Lambda 950). The solution was extracted carefully to avoid the deposit being involved and no centrifuge was used.

2.3. Mechanism analysis

The composition of the precipitation was confirmed by XRD, confocal micro-Raman spectroscopy (Renishaw inVia Reflex) and Fourier Transform Infrared Spectroscopy (NICOLET 6700). The surface morphologies of ribbons were observed by scanning electron microscopy (SEM, Hitachi S4800). The surface compositions of ribbons was also examined by energy dispersive spectroscopy (EDS) equipped on the SEM machine. The surface elemental information of ribbons was analyzed by X-ray photoelectron spectroscopy (XPS, AXIS Ultra DLD) with a monochromatic Al $K\alpha$ X-ray source ($h\nu$ = 1486.6 eV).
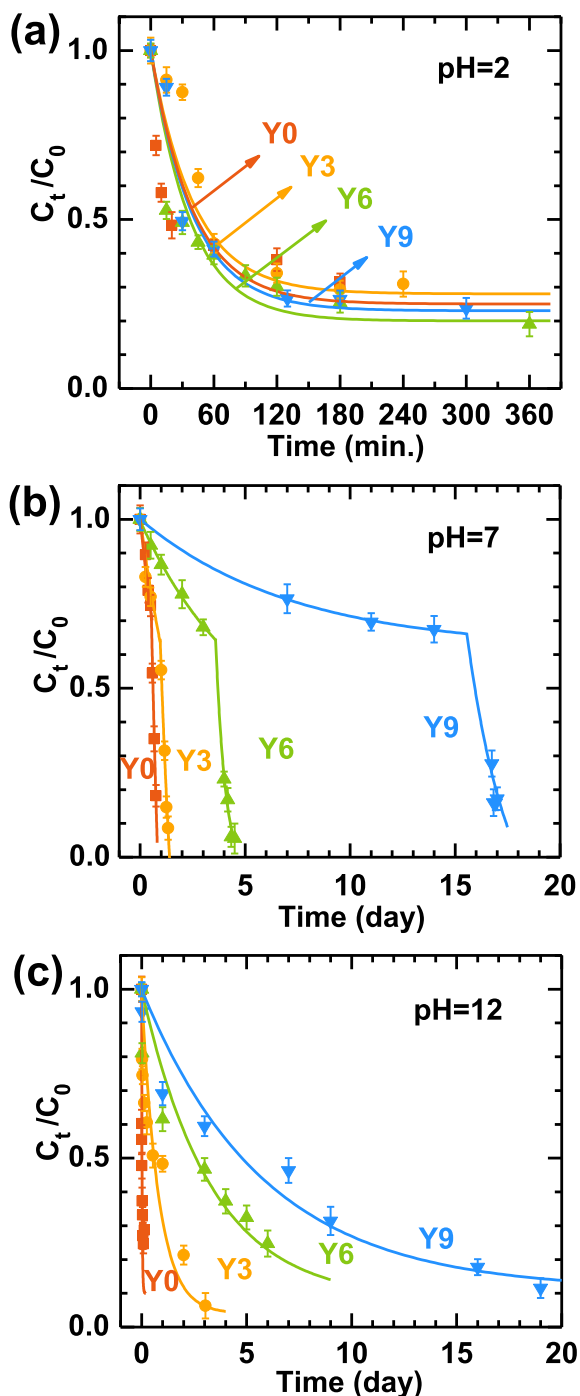

Fig. 3. The normalized concentration of DB 2B solutions along with reaction time for Al-Ni-Y ribbons of different Y content at room temperature. (a) pH = 2, (b) 7, and (c) 12.
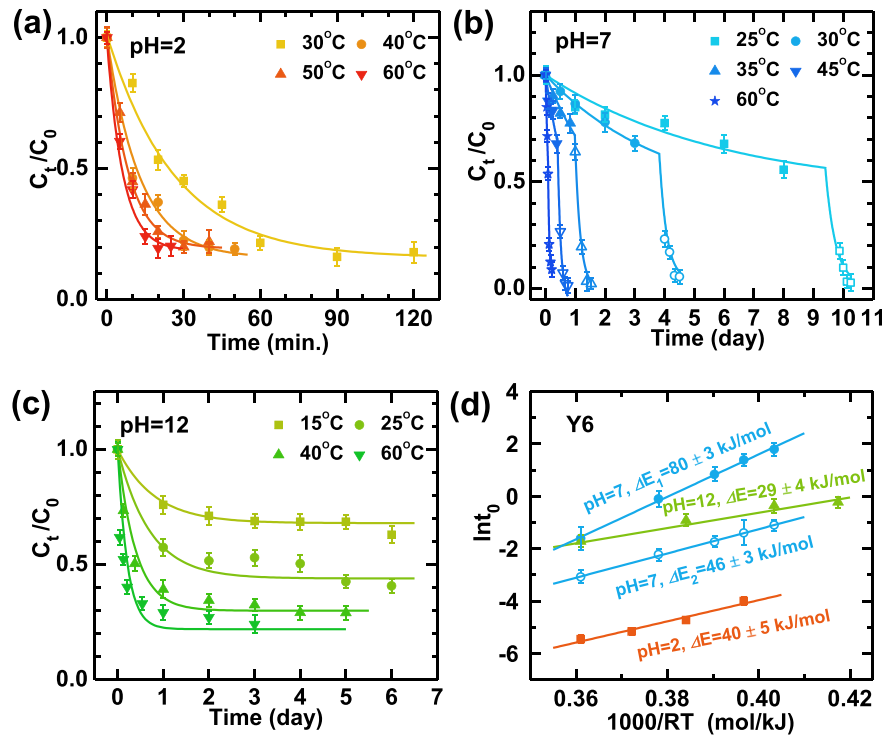
Fig. 4. The normalized concentration of DB 2B solutions after different reaction time with Y6 metallic glass ribbons at different temperatures for (a) pH = 2, (b) 7, and (c) 12, respectively. The curves are fitting results by $C = C_1 \exp(-t/t_0) + C_2$ (d) Plot of the reaction time (t_0) versus temperature. The solid lines are fitting results by $t_0 = \tau_0 \exp(\Delta E/RT)$.

3. Results

3.1. Atomic structure of the metallic ribbons

The atomic structure of Y0, Y3, Y6, Y9 ribbons was investigated by XRD and DSC. As shown in Fig. 1(a), for the Y-free ribbons, Bragg peaks corresponding to α-Al and Al$_3$Ni crystalline phases are found. For 3 at.% Y addition, however, the XRD curve exhibits a broad diffusive diffraction peak with a weak peak around 45° which denotes that the sample is mainly amorphous embedded with a little nanocrystalline α-Al. Further alloying with 6 at.% and 9 at.% Y, the XRD curves of the ribbons exhibit broad diffusive diffraction peak which confirms the amorphous nature of the ribbons. As shown in Fig. 1(b), the DSC curves exhibit obvious exothermic peaks which further verify the amorphous nature of the ribbons. The onset temperature of the first exothermic crystallization event, T_x, is marked by arrow. It is probably related to the precipitation of α-Al [44]. Y addition drives T_x to higher temperature indicating the enhancement of thermal stability and glass forming ability.

3.2. The reactivity in solutions with different pH

The azo dye wastewater is usually alkaline and some of them are acidic. Slightly change of solution pH can change the degradation efficiency greatly [45,46]. To evaluate the effects of solution pH on the decomposition process, the degradation experiments by Y6 metallic glass were carried out at pH = 2, 7, and 12. It is confirmed that the solutions are decoloured completely, as shown in Fig. 2(a). The UV absorption spectra are shown in Fig. 2(b)–(d). The characteristic absorption peak around 570 nm arises from −N═N− of DB 2B dye molecules. The intensity of the absorption peak is proportional to the concentration of azo dyes solution. Along with the degradation process, the intensity of the absorption peak decreases.

The change of normalized concentration of DB 2B solutions at pH = 2, 7, and 12 is shown in Fig. 2(e). The degradation process is fitted using a pseudo first-order reaction equation, $C = C_1 \exp(-t/t_0) + C_2$, where C is the normalized concentration of solution, C_1 and C_2 are fitting constants, t is reaction time, t_0 is degradation time constant. The comparison of t_0 at different pH solutions is shown in Fig. 2(f). For pH = 2, $t_0 = 39$ min. For pH = 7, the reaction is carried out in two stages. In the first stage, the reaction rate is rather slow, $t_0 = 5$ days. In the second stage, $t_0 = 2$ h. For pH = 12, $t_0 = 3.3$ days which is much faster compared to the first stage at pH = 7. Different from other alloys [8,25], the reactivity of Al-based metallic glasses increases by about 50% in alkaline solutions than that in neutral solutions. This is beneficial for application.

3.3. The influence of Y addition in the metallic glasses

Thanks to their nonequilibrium nature, the compositions of the metallic glasses can be widely tuned. It has been proved that small change of the components can change the physical and chemical properties greatly [47–49]. To understand the role of each element in the alloys during the degradation process, we tested the decoloration efficiency of Y0, Y3, Y6, Y9 metallic ribbons. For pH = 2, all the metallic ribbons can degrade azo dye in short time, as shown in Fig. 3(a). The degradation time constants are about 40, 42, 39, 41 min for Y0, Y3, Y6, Y9 ribbons, respectively. The degradation rate of the azo dye is not sensitive to the composition change of the ribbons. For pH = 7 and 12, the degradation rate decreases greatly with the replacement of Al with Y, as shown in Fig. 3(b) and (c). For pH = 7, the degradation time constants in the first stage are 1.6, 2.2, 5.0, 9.1 days for Y0, Y3, Y6, Y9 ribbons, respectively. Though the degradation time constants don't change much at the second stage, the onset time for the second stage increases from 13 h to 2, 4, 15 days for Y0, Y3, Y6, Y9 ribbons, respectively. For pH = 12, the degradation time constant is 35 min, 0.8 day, 3.3 day, 5.8 day for Y0,
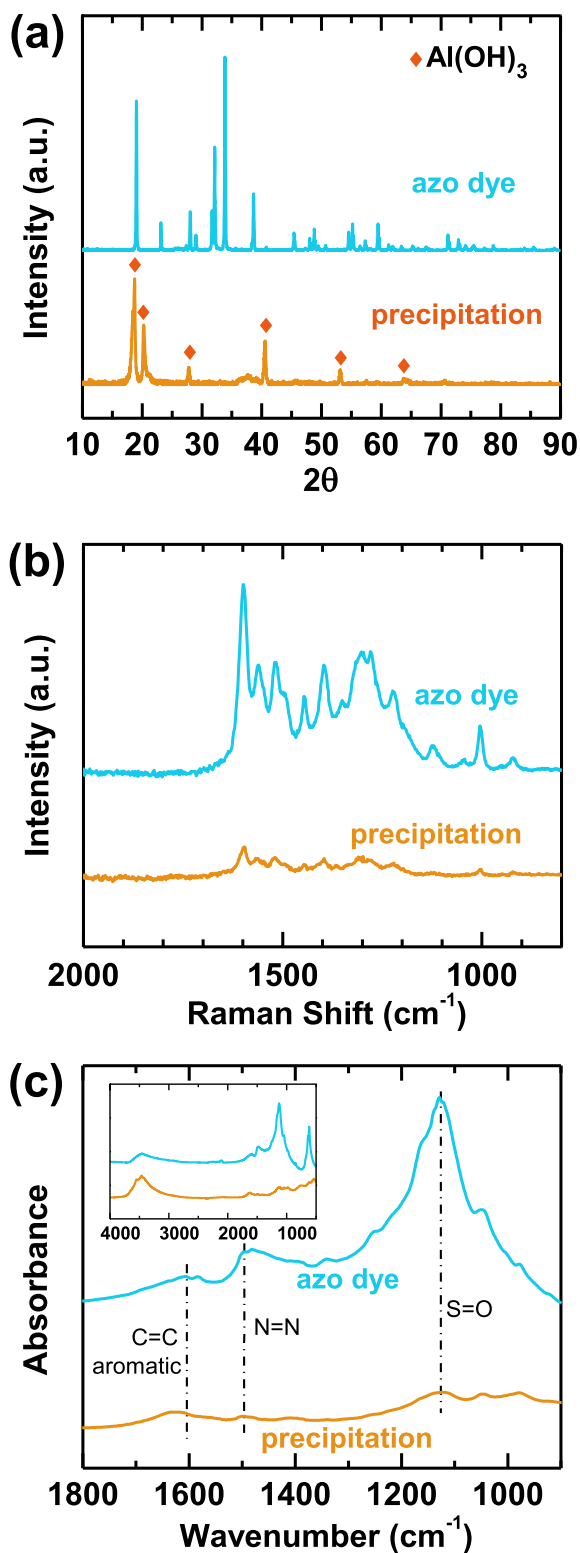
Fig. 5. (a) XRD curves, (b) Raman spectra, and (c) FTIR spectra of azo dye powders and precipitation after reaction in pH = 7 solution. Inset of (c) shows the whole FTIR spectrum from 4000 to 500 cm^{-1}.

Y3, Y6, Y9 ribbons, respectively. Thus, the degradation efficiency can be greatly enhanced by decreasing Y, especially for pH = 7 and 12. However, proper Y addition is necessary to get an amorphous structure, which can decreases the corrosion of the ribbons by water and maintain high decoloration efficiency for a long-life.

3.4. The reaction activation energy

The reaction activation energy is an important kinetic parameter to understand the mechanism of degradation process [50]. To determine the degradation activation energy, the reaction efficiency at different temperatures is evaluated, as shown in Fig. 4(a)–(c). The reaction activation energy (ΔE) can be evaluated with Arrhenius equation, $t_0 = \tau_0 \exp(\Delta E/RT)$, where τ_0 is a time pre-factor, R is the gas constant. The activation energy for Y6 metallic glass ribbons is determined to be 40 kJ/mol at pH = 2, 80 kJ/mol for the first stage at pH = 7, 46 kJ/mol for the second stage at pH = 7, and 29 kJ/mol at pH = 12, respectively, as shown in Fig. 4(d). The large ΔE for pH = 7 is consistent with the low reactivity as confirmed in Fig. 2(e). On the other hand, a large activation energy also denotes that the reactivity increases rapidly when temperature increases, which benefits their application at high temperatures.

4. Discussion

4.1. Two stage reaction

For pH = 7, accompanied with the production of blue precipitation in the second stage, the azo dye solution gets decolorized quickly and completely, as shown in Fig. 2(a). To understand the mechanism of the two stage reaction at pH = 7, we analyzed the compositions of the blue precipitation by XRD, Raman spectroscopy and Fourier Transform Infrared Spectroscopy (FTIR). The XRD pattern of the precipitation shows sharp Bragg peaks which can be indexed as the diffraction of Al(OH)$_3$, as shown in Fig. 5(a). This demonstrates that the precipitation is mainly Al(OH)$_3$. The Raman spectrum of the precipitation matches well with the DB 2B azo dye powders, and the intensity is pretty weak, as shown in Fig. 5(b). This indicates the existence of azo dye molecules. Furthermore, the FTIR spectra of azo dye powders and the precipitation are shown in Fig. 5(c). The band around 1496 cm^{-1} derives from the N=N bond (stretching vibration mode); the band around 1608 cm^{-1} derives from the C=C bond (aromatic, stretching vibration mode) [51]. For the precipitation, the band at 1496 cm^{-1} (N=N) becomes weaker compared to the band at 1625 cm^{-1} (aromatic C=C), which denotes the degradation of N=N bond. And blue shift from 1608 to 1625 cm^{-1} is observed for the band of aromatic C=C, which denotes that electrons transfer to the aromatic C=C after the break of N=N bond. In conclusion, the precipitation is mainly composed of Al(OH)$_3$ with adsorption of azo dye molecules and its byproducts. Thus, in the first stage, due to the coverage of oxide and the low concentration of H$^+$, only a small number of metals react with azo dye. The product of the first stage reaction, Al(OH)$_3$, transport into solution by convection effects. The Al(OH)$_3$ colloid particles are positively charged, [Al$_m$(OH)$_n$]$^{(3m-n)+}$ [52], which exhibit strong adsorption ability to the negatively charged azo dye molecules. This is responsible for the quick decoloration in the second stage. Because the generation of Al(OH)$_3$ colloid particles need incubation time, there is little precipitation in the first reaction stage. The precipitation time can be shortened greatly by decreasing Y or increasing the temperature. Over all, the decolorization of solutions is mainly attributed to the degradation by zero-valent metals, especially for pH = 2, 12 and the first reaction stage in pH = 7. While, for the second reaction stage in pH = 7, the decolorization of solutions is ascribed to both the degradation by zero-valent metals and adsorption by Al(OH)$_3$ colloid particles.

4.2. Surface morphology

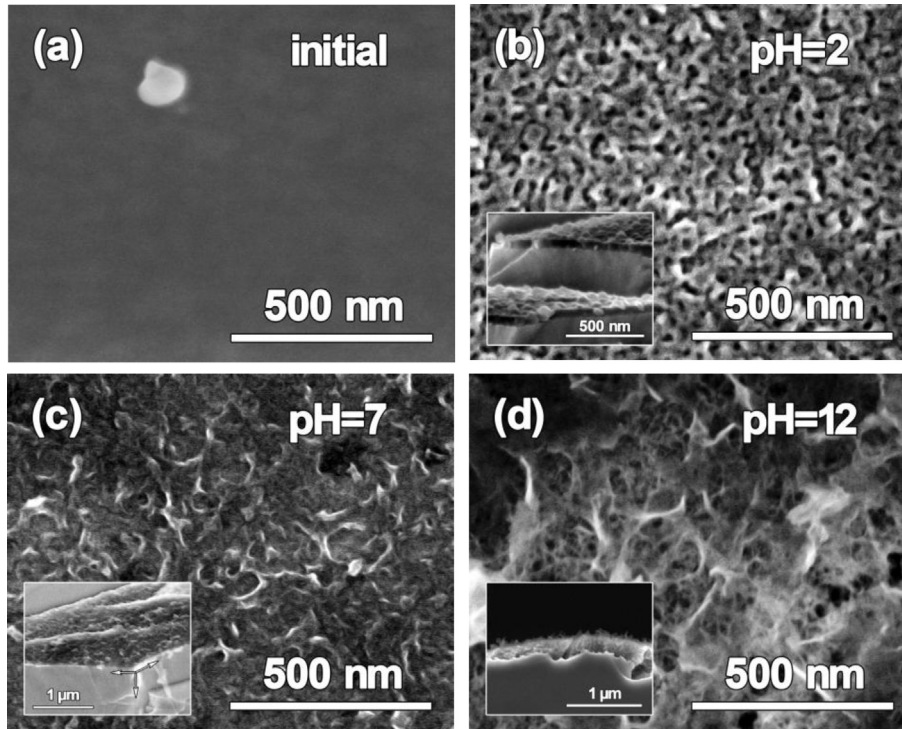To study the origin of the big kinetic difference in acidic, neutral

Fig. 6. Surface morphologies of Y6 ribbons before (a) and after reaction with DB 2B solutions at different pH values (b) pH = 2, (c) pH = 7, (d) pH = 12. Insets of (b), (c), and (d) are the side-view SEM images of the reacted ribbons. The thickness of reaction layers are about 50 nm, 80 nm, and 250 nm for pH = 2, 7, and 12, respectively.

and alkaline solutions, the surface morphologies for Y6 metallic glass ribbons before and after reaction were studied. For initial metallic glass ribbons, the surface is very smooth with a shining metallic color, as shown in Fig. 6(a). After reaction in pH = 2 solution, the surface is distributed with fine and uniform ligament-pore structure with pore size about 20 nm, which indicates compositional alteration during the reaction, as shown in Fig. 6(b). After reaction in pH = 7 solution, the surface roughness increases
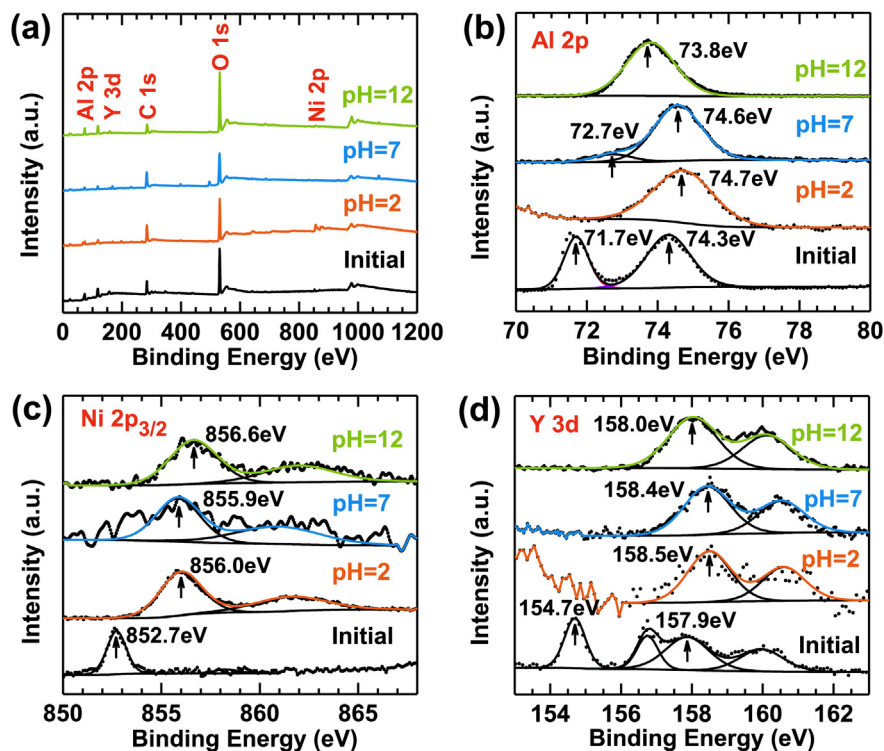

Fig. 7. X-ray photoelectron spectra of Y6 ribbons before and after reaction with DB 2B solutions. (a) The whole spectra, (b) Al 2p, (c) Ni 2p$_{3/2}$, and (d) Y 3d.

Table 1
Elemental information of Y6 ribbons before and after reaction with DB 2B solution by XPS.

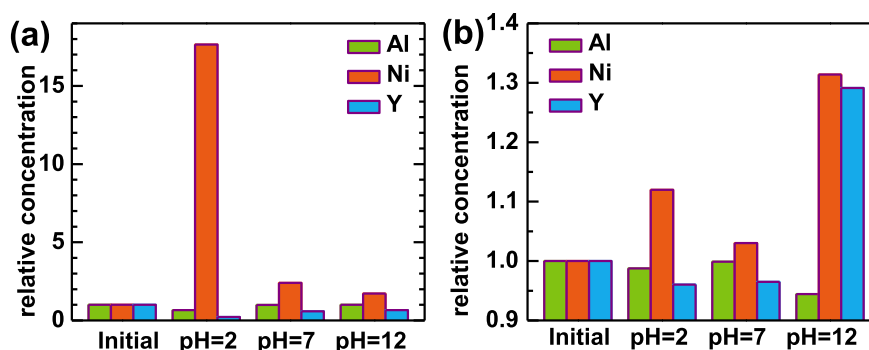| Conditions	Decomposition of XPS lines	Al 2p			Ni 2p$_{3/2}$		Y3d$_{5/2}$	
		Al^0	Al^{n+}	Al^{3+}	Ni^0	Ni^{n+}	Y^0	Y^{3+}
Initial	BE (eV)	71.7		74.3	852.7	...	154.7	157.9
	FWHM (eV)	0.80		1.47	1.15	...	0.69	1.45
	Ratio (at.%)	32.5		60.2	2.1	...	2.2	3.0
pH = 2	BE (eV)	...		74.7	...	856.0	...	158.5
	FWHM (eV)	...		1.95	...	2.49	...	1.42
	Ratio (at.%)	...		61.8	...	37.1	...	1.2
pH = 7	BE (eV)		72.7	74.6	...	855.9	...	158.4
	FWHM (eV)		1.29	1.57	...	2.65	...	1.52
	Ratio (at.%)		9.4	82.5	...	5.0	...	3.0
pH = 12	BE (eV)	...		73.8	...	856.6	...	158.0
	FWHM (eV)	...		1.61	...	2.85	...	1.64
	Ratio (at.%)	...		93.0	...	3.6	...	3.4

Fig. 8. The relative concentration of the component elements detected by (a) XPS and (b) EDS.

which confirms the reaction between the metallic glass ribbons and solution, as shown in Fig. 6(c). After reaction in pH = 12 solution, the surface becomes nanoporous due to the dealloying of Al by NaOH. The pore sizes is inhomogeneous ranging from 10 to 30 nm, which is different from the normal dealloying process [53], since the concentration of NaOH is pretty low (0.01 M). This may be because that the original pitting points can extend vertically and horizontally along with dealloying. The vertical extension is responsible for the formation of large pores, while the horizontal extension contributes to the exfoliation of oxide layer and the exposure of small pores, as shown in Fig. 6(d).

The cross section morphologies of ribbons were also studied to check the thickness of the reaction layer. For pH = 2, as shown in inset of Fig. 6(b) (a magnified shear "slip steps") [54], the thickness of nanoporous layer is only about 50 nm indicating the reaction product can easily exfoliate from the surface, and the zero valent metals can be exposed to solutions continuously to maintain the high reaction activity. For pH = 7, as shown in inset of Fig. 6(c), the thickness of reaction layer is about 80 nm indicating that the convection and electrostatic repulsion effects can avoid the deposition of Al(OH)$_3$. Thus, the ribbons can continuously release Al(OH)$_3$ to decolorize the solution in the second stage. For pH = 12, as shown in inset of Fig. 6(d), the thickness of nano-porous layer is about 250 nm, which much larger than that for pH = 2 and 7. The thick nano-porous structure can greatly increase the specific surface area, which is beneficial to the adsorption and reaction process. The nano-porous layer may storage [H] produced during the dealloying process to extend the reaction time of [H] and azo dyes. Furthermore, the Ni/Y enriched nano-porous structure and the amorphous matrix may form a micro-battery to accelerate the degradation process [33]. Based on the good properties from the

nano-porous structure, the reaction activity at pH = 12 is much higher than the first stage at pH = 7, which is different from other metallic glasses. The reaction activity at pH = 12 is lower than that at pH = 2, which is attributed to the repulsive interaction between the negatively charged surface and azo dye molecules [9].

4.3. Analysis of surface compositions

The chemical states and contents of the elements on the surface
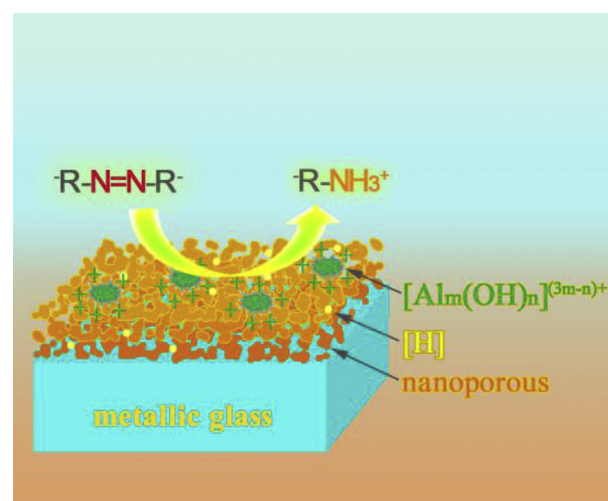

Fig. 9. A schematic illustration of the degradation of azo dyes on the surface of metallic glasses in alkaline solution.

of Y6 ribbons before and after reaction were investigated by XPS. Though some of the ribbons after reaction (especially at pH = 2 and 7) still keep a shining metallic color, the binding energy of Al 2p, Ni $2p_{3/2}$, Y 3d increases after reaction which indicates the oxidation of Al, Ni, Y, as can be seen from Fig. 7(b)–(d).

The elemental information from the outermost atomic layers is summarized in Table 1. Only metal elements are considered in this paper. Before reaction, the surface is a mixture of Al^0 (71.7 eV), Al_2O_3 (74.3 eV), Ni^0 (852.7 eV), Y^0 (154.7 eV), Y_2O_3 (157.9 eV). About 40% of the atoms are in zero valent states. The atomic ratio of Al: Ni: Y is 92.7: 2.1: 5.2, which is different from the nominal components (85: 9: 6). This is because Al and Y are easier to get oxidized than Ni during melt spinning (exotherm when reaction with O is −1678.2 kJ/mol for Al_2O_3, −1906.7 kJ/mol for Y_2O_3, −232.2 kJ/mol for NiO) [55] and aggregate on the surface of ribbons. Moreover, the reductive Al^0, Ni^0, and Y^0 were supposed to serve as the electron donors during the degradation process, while the aggregated inactive oxides slow down the decoloration efficiency. This is why the addition of Y decreases the reaction activity.

After reaction with azo dye solutions at pH = 2, the surface is probably a mixture of $AlCl_3$, Al_2O_3 (74.7 eV), $NiCl_2$, $NiOH_2$, Ni_2O_3 (856.0 eV), YCl_3, Y_2O_3 (158.5 eV). All of these products can be exfoliated and dissolved into the solution at such acidic condition, which is beneficial to expose the underlying reductive Al^0, Ni^0, and Y^0 atoms continuously to maintain high reaction efficiency. The change of the component elements on the surface after reaction was evaluated by the relative concentration, which is normalized by the initial state, as shown in Fig. 8. Both XPS and EDS results confirm that Ni increases while Al and Y decreases indicating that there is compositional selection.

After reaction with azo dye solutions at pH = 7, the surface is probably a mixture of AlO_x (72.7 eV), Al_2O_3, Al_2NiO_4, $Al(OH)_3$, AlOOH (74.6 eV), $Ni(OH)_2$, Ni_2O_3, Al_2NiO_4, NiOOH (855.9 eV), Y_2O_3 (158.4 eV). These products can be transported into the solution by convection effects. This promotes the continuous formation of $Al(OH)_3$ colloid particles, $[Al_m(OH)_n]^{(3m-n)+}$, which are positively charged and have strong adsorption ability to azo dye molecules. Both XPS and EDS results show that the content of Ni increases while Al and Y decrease indicating the selective reaction of Al and Y, as shown in Fig. 8. This is in accordance with the suspended precipitation of $Al(OH)_3$ and the rough surface morphology.

After reaction with azo dye solutions at pH = 12, the surface is covered by a mixture of $Al(OH)_3$, $Al_2O_3 \cdot 3H_2O$, $AlNiYO_x$ (73.8 eV), $Ni(OH)_2$, Al_2NiO_4, NiOOH (856.6 eV), Y_2O_3 (158.0 eV). There is no zero valent metal detected. The thick nano-porous structure benefits the adsorption and reaction process. Both XPS and EDS results confirm that the content of Ni increases, as shown in Fig. 8. This is consistent with the SEM result that a nano-porous Ni/Y structure forms after the dealloying of Al. Based on the morphology and elemental analysis, the degradation progress of azo dyes can be schematically illustrated in Fig. 9. Nano-porous Ni/Y forms on the surface of metallic glass due to the dealloying of Al. The thick nano-porous structure can enlarge surface area and may form a micro-battery with the amorphous matrix, which is beneficial to the adsorption and reaction of azo dyes and atomic hydrogen [H]. As the reaction is carried out, the solution pH decreases and the positively charged $[Al_m(OH)_n]^{(3m-n)+}$ may also form on the surface of nano-porous structure, which contribute to the strong adsorption to azo dyes and promotes the decolorization of azo dyes synergistically.

5. Conclusions

We find that Al-based metallic glass ribbons can decolorize DB 2B solutions at wide pH conditions via different mechanisms. For

pH = 2, due to the refreshing effect of H^+, the azo dye solution can be continuously degraded by metallic glass. For pH = 7, the reaction is carried out in two stages. At the first stage, the degradation is slower than pH = 2 and 12 due to the aggregation of Al_2O_3 and Y_2O_3 on surface. At the second stage, the decolorization efficiency becomes larger, because the produced colloid particles $[Al_m(OH)_n]^{(3m-n)+}$ are positively charged and exhibit excellent adsorption ability to azo dye molecules. For pH = 12, the degradation efficiency is higher than the first stage at pH = 7, which is different from other metallic glasses. The increased degradation efficiency is mainly attributed to the enlarged surface area and micro-battery effect caused by nano-porous structure after the dealloying of Al. And the activation energy of pH = 2 and 12 is lower than that of pH = 7 at the first stage. Suitable modification of alloy composition can further increase decoloring efficiency. These results suggest that the Al-based metallic glasses hold promising potential in degrading azo dyes solutions.

References

[1] S. Singh, M.D. Ediger, J.J. de Pablo, Ultrastable glasses from in silico vapour deposition, Nat. Mater. 12 (2013) 139–144.
[2] H.B. Yu, Y.S. Luo, K. Samwer, Ultrastable metallic glass, Adv. Mater. 25 (2013) 5904–5908.
[3] W.L. Johnson, Bulk amorphous metal—an emerging engineering material, JOM 3 (2002) 40–43.
[4] M.F. Ashby, A.L. Greer, Metallic glasses as structural materials, Scr. Mater. 54 (2006) 321–326.
[5] A. Inoue, A. Takeuchi, Recent development and application products of bulk glassy alloys, Acta Mater. 59 (2011) 2243–2267.
[6] M. Carmo, R.C. Sekol, S.Y. Ding, G. Kumar, J. Schroers, A.D. Taylor, Bulk metallic glass nanowire architecture for electrochemical applications, ACS Nano 5 (2011) 2979–2983.
[7] J.Q. Wang, Y.H. Liu, M.W. Chen, G.Q. Xie, D.V. Louzguine-Luzgin, A. Inoue, J.H. Perepezko, Rapid degradation of azo dye by Fe-based metallic glass powder, Adv. Funct. Mater. 22 (2012) 2567–2570.
[8] J.Q. Wang, Y.H. Liu, M.W. Chen, D.V. Louzguine-Luzgin, A. Inoue, J.H. Perepezko, Excellent capability in degrading azo dyes by MgZn-based metallic glass powders, Sci. Rep. 2 (2012) 00418–00423.
[9] Y. Tang, Y. Shao, N. Chen, X. Liu, S.Q. Chen, K.F. Yao, Insight into the high reactivity of commercial Fe–Si–B amorphous zero-valent iron in degrading azo dye solutions, RSC Adv. 5 (2015) 34032–34039.
[10] B. Zberg, P.J. Uggowitzer, J.F. Loffler, MgZnCa glasses without clinically observable hydrogen evolution for biodegradable implants, Nat. Mater. 8 (2009) 887–891.
[11] J. Schroers, G. Kumar, T.M. Hodges, S. Chan, T.R. Kyriakides, Bulk metallic glasses for biomedical applications, JOM 61 (2009) 21–29.
[12] X. Gu, Y. Zheng, S.P. Zhong, T.F. Xi, J.Q. Wang, W.H. Wang, Corrosion of, and cellular responses to Mg-Zn-Ca bulk metallic glasses, Biomaterials 31 (2010) 1093–1103.
[13] H.J. Yu, J.Q. Wang, X.T. Shi, D.V. Louzguine-Luzgin, H.K. Wu, J.H. Perepezko, Ductile biodegradable Mg-based metallic glasses with excellent biocompatibility, Adv. Funct. Mater. 23 (2013) 4793–4800.
[14] Y.H. Liu, J. Padmanabhan, B. Cheung, J.B. Liu, Z. Chen, B.E. Scanley, D. Wesolowski, M. Pressley, C.C. Broadbridge, S. Altman, U.D. Schwarz, T.R. Kyriakides, J. Schroers, Combinatorial development of antibacterial Zr-Cu-Al-Ag thin film metallic glasses, Sci. Rep. 6 (2016) 26950–26957.
[15] C. Zhang, W.B. Bu, D.L. Ni, S.J. Zhang, Q. Li, Z.W. Yao, J.W. Zhang, H.L. Yao, Z. Wang, J.L. Shi, Synthesis of iron nanometallic glasses and their application in cancer therapy by a localized Fenton reaction, Angew. Chem. Int. Ed. 55 (2016) 2101–2106.
[16] T. Egami, Magnetic amorphous alloys: physical and technological applications, Rep. Prog. Phys. 47 (1984) 1601–1725.
[17] M.X. Zhang, F.L. Kong, A.D. Wang, C.T. Chang, B.L. Shen, Soft magnetic properties of bulk FeCoMoPCBSi glassy core prepared by copper mold casting, J. Appl. Phys. 111 (2012) 07A312–307A315.
[18] W.H. Wang, Bulk metallic glasses with functional physical properties, Adv.

Mater. 21 (2009) 4524–4544.

[19] J.T. Huo, L.S. Huo, H. Men, X.M. Wang, A. Inoue, J.Q. Wang, C.T. Chang, R.W. Li, The magnetocaloric effect of Gd-Tb-Dy-Al-M (M = Fe, Co and Ni) high-entropy bulk metallic glasses, Intermetallics 58 (2015) 31–35.

[20] C.Q. Zhang, H.F. Zhang, M.Q. Lv, Z.Q. Hu, Decolorization of azo dye solution by Fe−Mo−Si−B amorphous alloy, J. Non Cryst. Solids 356 (2010) 1703–1706.

[21] C.Q. Zhang, Z.W. Zhu, H.F. Zhang, Z.Q. Hu, Rapid reductive degradation of azo dyes by a unique structure of amorphous alloys, Chin. Sci. Bull. 56 (2011) 3988–3992.

[22] N.K. Amin, Removal of Direct Blue-106 dye from aqueous solution using new activated carbons developed from pomegranate peel: adsorption equilibrium and kinetics, J. Hazard. Mater. 165 (2009) 52–62.

[23] W.X. Zhang, C.B. Wang, H.L. Lien, Treatment of chlorinated organic contaminants with nanoscale bimetallic particles, Catal. Today 40 (1998) 387–395.

[24] S.D. Kalme, G.K. Parshetti, S.U. Jadhav, S.P. Govindwar, Biodegradation of benzidine based dye Direct Blue-6 by pseudomonas desmolyticum NCIM 2112, Bioresour. Technol. 98 (2007) 1405–1410.

[25] Y. Tang, Y. Shao, N. Chen, K.F. Yao, Rapid decomposition of Direct Blue 6 in neutral solution by Fe−B amorphous alloys, RSC Adv. 5 (2015) 6215–6221.

[26] S.H. Xie, P. Huang, J.J. Kruzic, X.R. Zeng, H.X. Qian, A highly efficient degradation mechanism of methyl orange using Fe-based metallic glass powders, Sci. Rep. 6 (2016) 21947–21956.

[27] P. Liu, J.L. Zhang, M.Q. Zha, C.H. Shek, Synthesis of an Fe rich amorphous structure with a catalytic effect to rapidly decolorize azo dye at room temperature, ACS Appl. Mater. Interfaces 6 (2014) 5500–5505.

[28] Y.F. Zhao, J.J. Si, J.G. Song, Q. Yang, X.D. Hui, Synthesis of Mg−Zn−Ca metallic glasses by gas-atomization and their excellent capability in degrading azo dyes, Mater. Sci. Eng. B 181 (2014) 46–55.

[29] M. Iqbal, W.H. Wang, Synthesis and characterization of Mg-based amorphous alloys and their use for decolorization of azo dyes, in: IOP Conference Series: Mater. Sci. Eng, vol. 60, 2014, p. 012035.

[30] M. Ramya, M. Karthika, R. Selvakumar, B. Raj, K.R. Ravi, A facile and efficient single step ball milling process for synthesis of partially amorphous Mg-Zn-Ca alloy powders for dye degradation, J. Alloys Compd. 696 (2017) 185–192.

[31] X.D. Qin, Z.W. Zhu, G. Liu, H.M. Fu, H.W. Zhang, A.M. Wang, H. Li, H.F. Zhang, Ultrafast degradation of azo dyes catalyzed by cobalt-based metallic glass, Sci. Rep. 5 (2015) 18226–18233.

[32] S. Das, S. Garrison, S. Mukherjee, Bi-functional mechanism in degradation of toxic water pollutants by catalytic amorphous metals, Adv. Eng. Mater. 18 (2016) 214–218.

[33] X.K. Luo, R. Li, J.Z. Zong, Y. Zhang, H.F. Li, T. Zhang, Enhanced degradation of azo dye by nanoporous-copper-decorated Mg−Cu−Y metallic glass powder through dealloying pretreatment, Appl. Surf. Sci. 305 (2014) 314–320.

[34] Z. Deng, C. Zhang, L. Liu, Chemically dealloyed MgCuGd metallic glass with enhanced catalytic activity in degradation of phenol, Intermetallics 52 (2014) 9–14.

[35] D.J. Wang, Z.H. Li, M.A. Rahman, J. Shen, Nanosized metal oxide and nanobelts prepared by selective dealloying of Ti-based amorphous powders, Langmuir 29 (2013) 8108–8115.

[36] J.F. Yang, X.F. Bian, M.L. Yuan, Y.W. Bai, Y. Liu, J.P. Fan, X.Q. Lu, K.K. Song, Excellent degradation performance of azo dye by metallic glass/titanium dioxide composite powders, J. Sol. Gel Sci. Technol. 67 (2013) 362–367.

[37] J.F. Yang, X.F. Bian, Y.W. Bai, X.Q. Lv, P. Wang, Rapid organism degradation function of Fe-based alloys in high concentration wastewater, J. Non Cryst.

Solids 358 (2012) 2571–2574.

[38] X.F. Wang, Y. Pan, Z.R. Zhu, J.L. Wu, Efficient degradation of Rhodamine B using Fe-based metallic glass catalyst by Fenton-like process, Chemosphere 117 (2014) 638–643.

[39] Z. Jia, J. Kang, W.C. Zhang, W.M. Wang, C. Yang, H. Sun, D. Habibi, L.C. Zhang, Surface aging behaviour of Fe-based amorphous alloys as catalysts during heterogeneous photo Fenton-like process for water treatment, Appl. Catal. B: Environ. 204 (2017) 537–547.

[40] Z. Jia, S.X. Liang, W.C. Zhang, W.M. Wang, C. Yang, L.C. Zhang, Heterogeneous photo Fenton-like degradation of cibacron brilliant red 3B-A dye using amorphous Fe78Si9B13 and Fe73.5Si13.5B9Cu1Nb3 alloys: the influence of adsorption, J. Taiwan Inst. Chem. Eng. 71 (2017) 128–136.

[41] Z. Jia, W.C. Zhang, W.M. Wang, D. Habibi, L.C. Zhang, Amorphous Fe78Si9B13 alloy: an efficient and reusable photo-enhanced Fenton-like catalyst in degradation of cibacron brilliant Red 3B-A dye under UV−vis light, Appl. Catal. B: Environ. 192 (2016) 46–56.

[42] Z. Jia, X.G. Duan, W.C. Zhang, W.M. Wang, H.Q. Sun, S.B. Wang, L.C. Zhang, Ultra-sustainable Fe78Si9B13 metallic glass as a catalyst for activation of persulfate on methylene blue degradation under UV-Vis light, Sci. Rep. 6 (2016) 38520–38529.

[43] Z.Y. Lv, X.J. Liu, B. Jia, H. Wang, Y. Wu, Z.P. Lu, Development of a novel high-entropy alloy with eminent efficiency of degrading azo dye solutions, Sci. Rep. 6 (2016) 34213–34223.

[44] J.Q. Wang, Y.H. Liu, S. Imhoff, N. Chen, D.V. Louzguine-Luzgin, A. Takeuchi, M.W. Chen, H. Kato, J.H. Perepezko, A. Inoue, Enhance the thermal stability and glass forming ability of Al-based metallic glass by Ca minor-alloying, Intermetallics 29 (2012) 35–40.

[45] J.A. Mielczarski, G.M. Atenas, E. Mielczarski, Role of iron surface oxidation layers in decomposition of azo-dye water pollutants in weak acidic solutions, Appl. Catal. B Environ. 56 (2005) 289–303.

[46] L. Liu, F.B. Li, C.H. Feng, X.Z. Li, Microbial fuel cell with an azo-dye-feeding cathode, Appl. Microbiol. Biotechnol. 85 (2009) 175–183.

[47] Y.H. Liu, G. Wang, R.J. Wang, D.Q. Zhao, M.X. Pan, W.H. Wang, Super plastic bulk metallic glasses at room temperature, Science 315 (2007) 1385–1388.

[48] W.L. Johnson, J. Plummer, Is metallic glass poised to come of age? Nat. Mater. 14 (2015) 553–555.

[49] L.C. Zhang, J. Xu, Glass-forming ability of melt-spun multicomponent (Ti, Zr, Hf)−(Cu, Ni, Co)−Al alloys with equiatomic substitution, J. Non Cryst. Solids 347 (2004) 166–172.

[50] G. Rothenberg, Catalysis: Concepts and Green Applications, Wiley, 2008.

[51] A. Mohammadi, M. Safarnejad, Synthesis, structural characterization and tautomeric properties of some novel bis-azo dyes derived from 5-arylidene-2,4-thiazolidinone, Spectrochim. Acta Part A 126 (2014) 105–111.

[52] C.A. Martínez-Huitle, E. Brillas, Decontamination of wastewaters containing synthetic organic dyes by electrochemical methods: a general review, Appl. Catal. B Environ. 87 (2009) 105–145.

[53] H.J. Qiu, J.Q. Wang, P. Liu, Y. Wang, M.W. Chen, Hierarchical nanoporous metal/metal-oxide composite by dealloying metallic glass for high-performance energy storage, Corros. Sci. 96 (2015) 196–202.

[54] C.A. Schuh, T.C. Hufnagel, U. Ramamurty, Mechanical behavior of amorphous alloys, Acta Mater. 55 (2007) 4067–4109.

[55] R. Jindal, V.S. Raja, M.A. Gibson, M.J. Styles, T.J. Bastow, C.R. Hutchinson, Effect of annealing below the crystallization temperature on the corrosion behavior of Al−Ni−Y metallic glasses, Corros. Sci. 84 (2014) 54–65.